Title

Gauging the feasibility of a downhole energy harvesting system through a proof-of-concept study

Authors

Kjolsing, Eric
Todd, Michael

Publication Date

2016-04-15

DOI

10.1117/12.2219313

Peer reviewed

Gauging the feasibility of a downhole energy harvesting system through a proof-of-concept study

Eric Kjolsing*[a], Michael Todd[a]
[a]Structural Engineering Department; University of San Diego, California
9500 Gilman Drive, Mail Code 0085, La Jolla, CA 92093-0085

ABSTRACT

Hydrocarbon well operators deploy downhole reservoir monitoring equipment in order to optimize the rate at which hydrocarbons are extracted. Alternative power sources are sought that could be deployed in these harsh environments to replace or supplement standard power sources currently in use. To this end, a three phase proof-of-concept study was performed to gauge the feasibility of such a device. In the first phase a parametric study was performed to understand how high uncertainty variables affect the natural frequency of a producing hydrocarbon well. In a follow up study, the relationship between boundary conditions and system damping was investigated. In the second phase a structural housing was designed to satisfy American Petroleum Institute load cases. Using finite element models and standard tube/casing geometries, design pressures were iterated until a permissible housing design was achieved. This preliminary design provided estimates of the radial width and volume in which energy harvesting and storage elements may be situated. In the last phase a software program was developed to estimate the energy that might be harvested from user specified harvester configurations. The program is dependent on user input production tube accelerations; this permits well operators to use well-specific vibrational data as inputs to generate well-specific energy output estimates. Results indicate that a downhole energy harvesting tool is structurally feasible under reasonable operating conditions but no conclusions can be made as to the sufficiency of generated power as no in-situ acceleration time histories are available. Future work is discussed. Approved for publication, LA-UR-16-21193.

Keywords: Energy Harvesting, Flow-Induced Vibration, Hydrocarbon Production, Oil Well, Hydrodynamic Function, Spectral Element Method, Fluid Conveying Pipe, Piezoelectric

1. INTRODUCTION

Downhole monitoring equipment may be deployed in producing wells to facilitate the optimal production of hydrocarbons. This equipment is typically powered by finite-life battery systems or conductor cable strung from the ground surface to the monitoring equipment. Recent interest has sparked investigations as to the feasibility of replacing or supplementing existing power sources with novel energy harvesting systems. By capturing ambient vibrations adjacent to the monitoring equipment, it may be possible to reduce the cost of supplying power and/or increase the life-span of the power source. While there are a number of patents utilizing various conceptual designs, there is little information available as to the actual feasibility of a downhole energy harvester. To the best of the authors' collective knowledge, the most advanced study was undertaken by Tubel Technologies in 2002, where they developed, fabricated, and tested a downhole power generating tool. Unfortunately, what little information was published from that study does not necessarily help current researchers and engineers in the development of other downhole harvesting tools.

The purpose of this manuscript is to document preliminary investigations as to the feasibility of a downhole energy harvesting system. Each investigation advances the reader's ability to design a downhole energy harvesting system and includes (a) characterizing a well's dynamic behavior, (b) a preliminary tool design, and (c) software enabling the estimation of harvestable energy. The envisioned well geometry is shown in Figure 1.

* eric.kjolsing@gmail.com

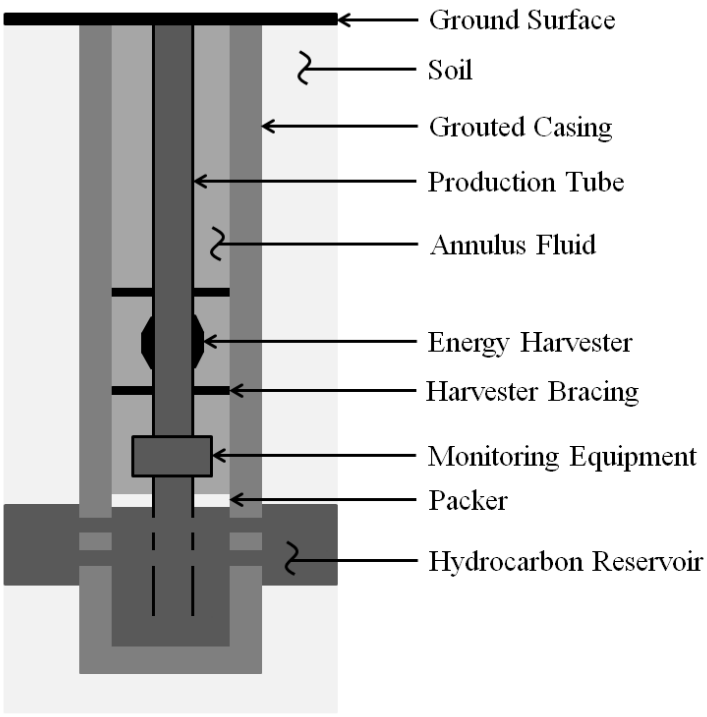

Figure 1. Well configuration

2. WELL CHARACTERIZATION

In most commonly utilized configurations piezoelectric energy harvesters are excited by base motions, resulting in induced strains across the piezoelectric elements which generate electrical charges that can be harvested. The base motions driving the piezoelectric element are then an important variable in determining how much energy can be harvested. In the current feasibility study the piezoelectric harvester is assumed fixed to the hydrocarbon production tube. As such, the dynamic behavior of the production tube must be understood as the driving base motion will be colored by the natural frequency of the production tube and the amplitude of motion will be limited by the amount of damping in the system.

In this section, two previous studies are summarized[1],[2]. Both utilized a hydrodynamic forcing function in an Euler-Bernoulli based equation of motion to model the behavior of a braced pipe conveying fluid. The spectral element method[3],[4] was used to determine the natural frequency and damping ratio for a number of configurations by varying those variables thought to have high uncertainty.

2.1 Natural frequency

In a 2015 study, Kjolsing and Todd[1] performed a parametric study to demonstrate how axial force, conveyed fluid velocity, and annulus fluid affects the first natural frequency of a fixed-fixed fluid-conveying pipe surrounded by a coaxial viscous fluid. The linearized equation of motion was written as[5]

$$E^*I\dot{w}'''' + EIw'''' + \{M_iU^2 - \bar{T} + \bar{p}A_i(1-2\nu)\}w'' + 2M_iU\dot{w}' + (M_i+m)gw' + c\dot{w} + (M_i+m)\ddot{w} - f_{hydro} = 0, \quad (1)$$

where

$$f_{hydro} = -i\rho_e\pi d^2\omega\Gamma U_0 e^{i\omega t} \quad (2)$$

represents the hydrodynamic forcing generated by the annulus fluid[6-8]. The remaining terms in equation (1) include: Kelvin-Voigt dissipation, flexural restoring force, centrifugal force, applied tension, pressure induced tension, Coriolis force, gravity, viscous damping, and inertia. The study compared fourteen cases with the variables of interest being: externally applied tension ($\bar{T}$), the conveyed fluid velocity (U), the annulus fluid density (ρ_e), and the hydrodynamic function (Γ) which is defined by the ratio of the conveying pipe outer radius to the grouted casing inner radius (d/D) and the annulus fluid viscosity (υ_e). The study concluded the following:

a. Much like a beam under axial load, including an external compression (or tension) in the system decreases (or increases) the real part of the natural frequency; the fluid velocity at which divergence occurs is shifted.
b. Increasing the conveyed fluid velocity decreases the real part of the natural frequency until bifurcation. This behavior is attributed to the centrifugal force which has the effect of inducing compression in the conveying pipe.
c. The annulus fluid density scales the effect of the hydrodynamic function.
d. The real part of the hydrodynamic function contributes an added mass to the system which lowers the real part of the natural frequency. Since divergence is a static phenomenon it does not depend on inertial changes, therefore, the fluid velocity at which divergence occurs does not change.
e. The imaginary part of the hydrodynamic function contributes viscous drag to the system causing a shift in both the real and imaginary parts of the natural frequency. Although the fluid velocity at which divergence occurs does not change, the bifurcation velocity does see a shift.

The inputs used in each case can be found in the referenced study, along with plots of natural frequency versus conveyed fluid velocity which demonstrate the aforementioned findings.

2.2 Damping

In a 2016 study, Kjolsing and Todd[2] investigated how changing the model's rotational boundary stiffness affected damping. Where the 2015 study assumed the rotational boundaries were fixed, the 2016 study introduced elastic springs allowing the model to represent some degree of flexibility in the pipe boundaries. The variables investigated were: the rotational boundary springs (K_r), the velocity of the conveyed fluid (U) and the viscosity of the annulus fluid (υ_e). Using the same equation of motion (equations (1) and (2)), the spectral element method was used to determine the natural frequency of the system. For a known natural frequency, the frequency-dependent hydrodynamic function could be explicitly determined. The damping ratio (specifically stemming from the viscous annulus fluid) was then found as[8]

$$\zeta = \frac{-\rho_e \pi d^2 \Gamma_i}{2(\Gamma_r \rho_e \pi d^2 + m + M_i)}. \tag{3}$$

The study found that, due to the frequency dependence of the hydrodynamic function, those systems with higher natural frequencies or lower annulus fluid viscosities resulted in lower damping ratios. The following conclusions were drawn:

a. Increasing the stiffness of the rotational boundary springs decreased the damping ratio.
b. Increasing the conveyed fluid velocity increased the damping ratio.
c. Increasing the annulus fluid viscosity increased the damping ratio.

The study provided both two- and three-dimensional visualizations relating boundary stiffness, conveyed fluid velocity, and damping ratios. The study concluded with a quantitative example illustrating the potential errors that might arise if the variables of interest are misestimated during the design of an energy harvester.

3. STRUCTURAL HOUSING

Having characterized the dynamic behavior of the production tube, a preliminary structural housing design was required as the maximum width and volume of the structural housing must be known to properly size the energy harvesting elements. Within the structural housing will reside the piezoelectric energy harvesting elements, required circuitry, and power storage devices. After considering the necessary fabrication sequence, an initial configuration was selected (shown in Figure 2). The structural housing is envisioned to be a modified length of standard tubing where larger diameter lengths of production tubing or casing provide a coaxial cavity in which the harvesting device will be placed.

A 3.5in diameter production tube geometry was assumed for preliminary design. Two housing lengths were considered: a 6in housing (matching the length of the drift mandrel) and a 24in housing (corresponding to an arbitrarily long

housing). For each geometry, a larger diameter coaxial length of pipe was selected based on an assumed casing inner diameter and necessary construction clearance requirements. Each housing was analyzed for a targeted design pressure of 5ksi, 10ksi, and 15ksi; higher strength steel grades were used in an attempt to withstand the higher design pressures. A minimum axial load (both tension and compression) was considered in each case to account for induced loads incurred during the setting of the packer. The load cases were taken from American Petroleum Institute Bulletin 5C3[9] and included bursting, collapse, and combined loading (i.e. Von Mises stress criteria). Finite element models were generated to analyze the critical stress locations (see Figure 2) which occurred at the internal or external fillet, depending on the given load case. The housing geometry (specifically the pipe wall thicknesses and fillet geometries) was iterated until a satisfactory design was reached. In most cases, the targeted design pressure was not sustainable so a reduced design pressure was considered.

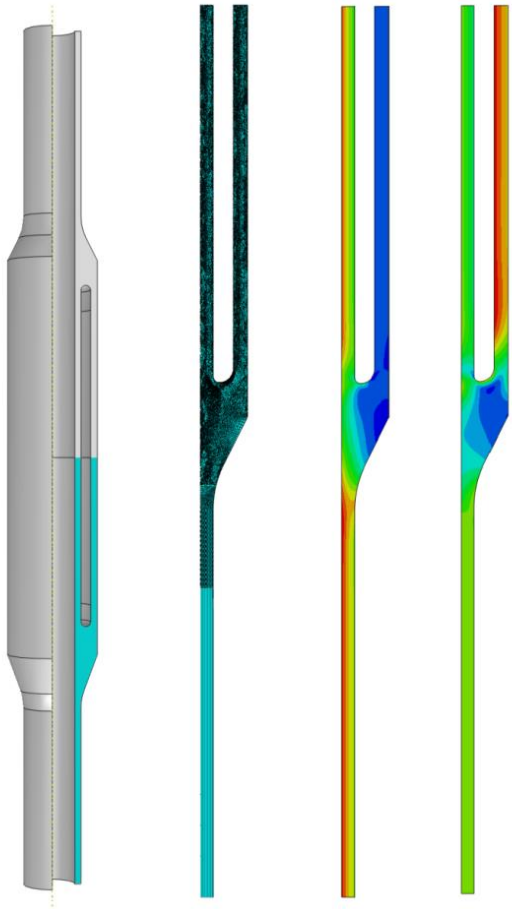

Figure 2. Structural housing. From left to right: 3/4 model rendering, refined mesh, Von Mises stress outputs

The preliminary design resulted in estimates of the radial width of the cavity and showed that the length of the housing can be unbounded within physical constraints. The available radial width varied between 0.49in and 0.68in after accounting for both force and thermal deformations. While the housing design could be further optimized, the radial widths found in the preliminary design are a reasonable lower bound.

4. POWER ESTIMATES

A MATLAB program was written to estimate the power output a given energy harvester configuration could generate. The program is structured in two phases. The first phase calculates optimal harvester natural frequencies for a user-specified configuration and produces an order of magnitude power estimate based on limited user information. The

second phase (described in section 5) generates an improved power estimate but requires significantly more user input. The program is generalized to allow well-specific analysis.

4.1 Phase one – order of magnitude power estimate

Phase one calculates optimal harvester natural frequencies and produces an order of magnitude power estimate. The preliminary power estimate is based on a single degree of freedom viscous damping model.

4.1.1 Inputs

The first phase is intended to provide an order of magnitude power estimate based on limited user input. By limiting the user input, a power estimate can be generated with minimal resources/user effort. If the generated power appears sufficient to meet the user's needs, a more in-depth analysis is performed (phase two). The required inputs include:

a. *Representative acceleration time histories of the production tube, at the elevation of the energy harvester, in the x-, y-, and z-directions.* The time histories may be taken from producing wells or artificially created to represent the expected downhole environment. Pre-processing may be needed to account for possible non-stationary effects, or alternatively, the program can be discretized into quasi-stationary time increments.

b. *A schedule of expected operating temperatures and the time frames over which the acceleration time histories ('a' above) appropriately characterize the production tubes vibration response (see Figure 3).* The well may see changes in the operating temperature and production tube acceleration profiles during secondary and tertiary recoveries.

c. *The window of time the user wants to optimize the total power output.* The user may be interested in maximizing the power output during the entire life of the well or, perhaps, for only a short window of time (e.g. for several months in the third year of production).

d. *The number, angular location, and orientation of each energy harvester.* The user can specify the location of harvester elements to create space for circuitry and storage elements.

e. *A table defining the dependence of the effective Young's Modulus of the piezoelectric element on time and temperature (see Figure 4).* Changes in the operating temperature and time-based degradation of the energy harvester will lead to changes in the harvester stiffness and, subsequently, to changes in the natural frequency of the harvester.

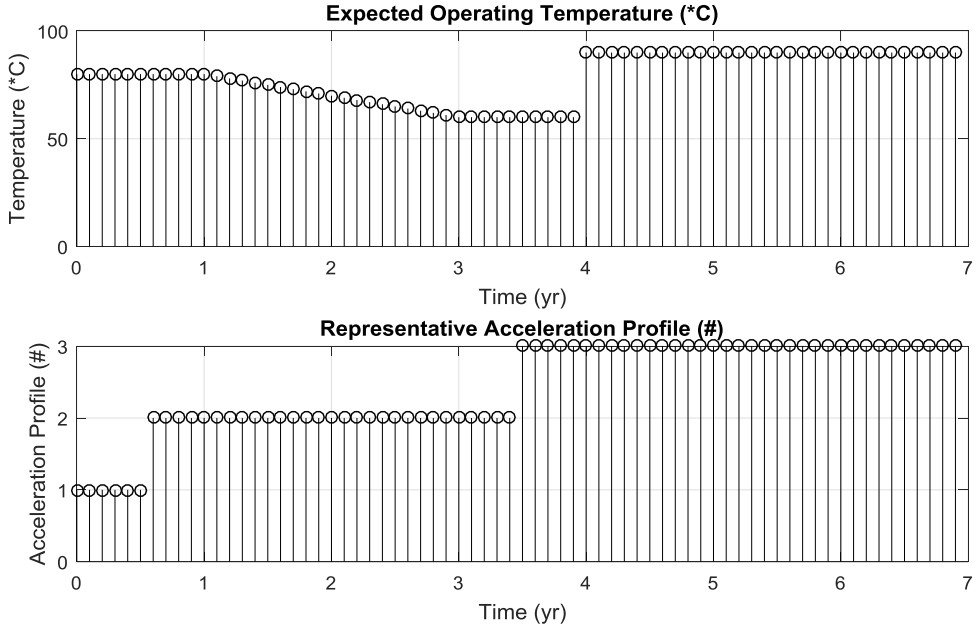

Figure 3. Expected operating schedule

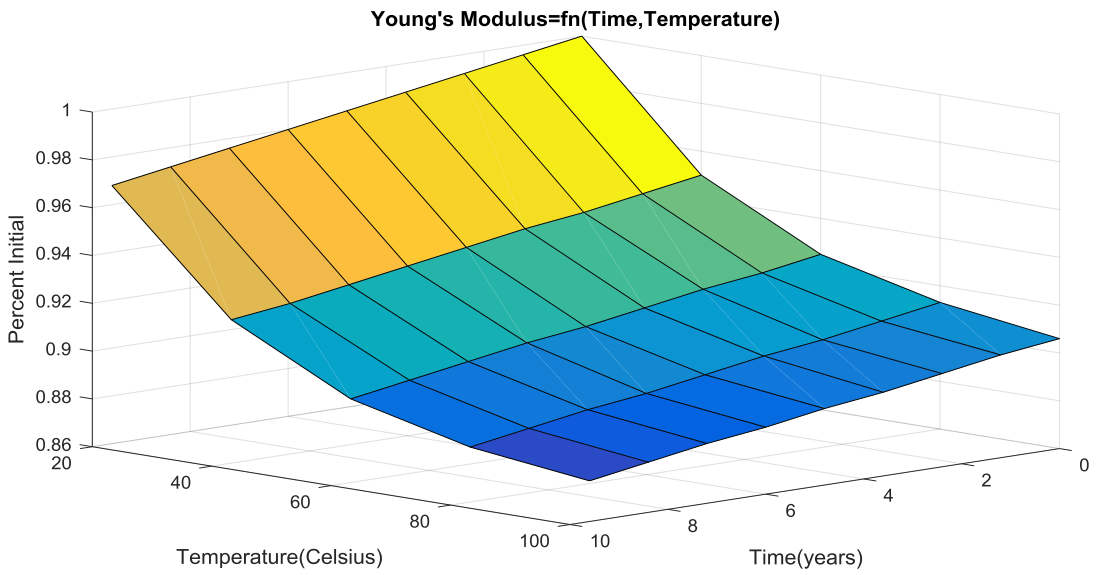

Figure 4. Time- and temperature-dependent changes in Young's Modulus

4.1.2 Program operations and outputs

The following discussion is limited to normally oriented energy harvesters (capturing a_{normal}) excited by vibrations orthogonal to the longitudinal axis of the production tube (see Figure 5). Similar calculations are performed for tangentially oriented harvesters and harvesters capturing vibrations along the axis of the production tube but are not included for brevity.

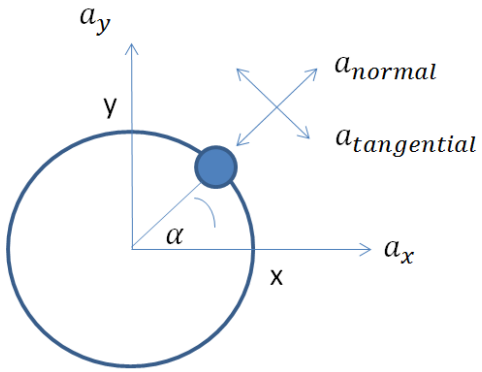

Figure 5. A simplified section of the energy harvester with a single harvesting element shown

For each acceleration profile, the program converts the x- and y-axis acceleration time histories into normally oriented time histories in 10° increments from 0° to 350°. Power spectrums are developed for these thirty-six time histories using Welch's method of overlapping segments. These spectrums are used to generate a three-dimensional angle-based power spectrum as shown in Figure 6.

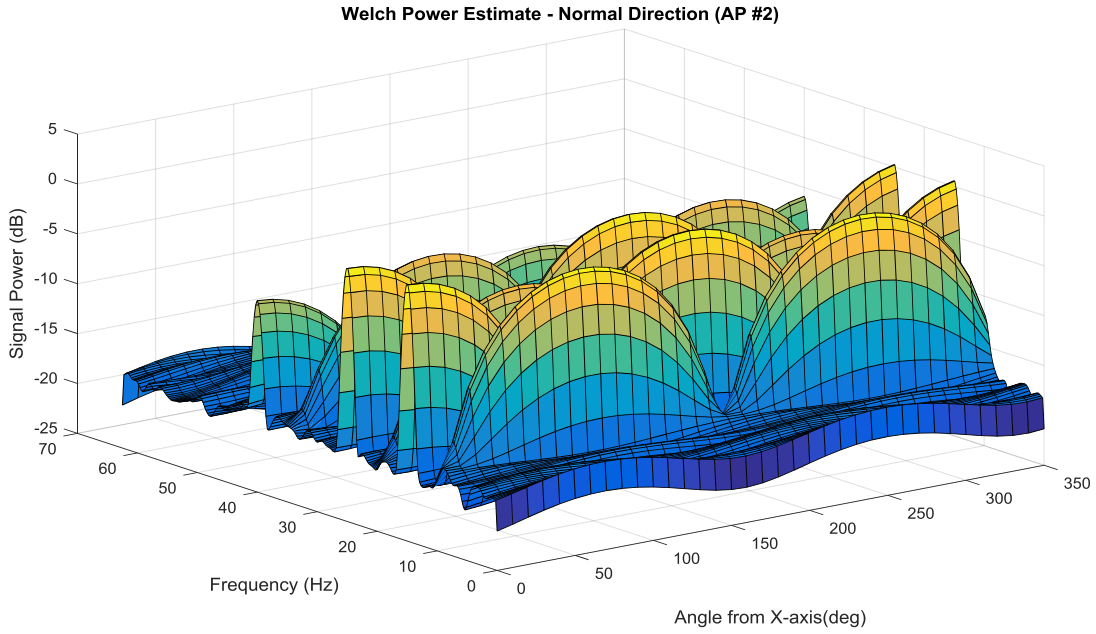

Figure 6. Three dimensional power spectrum

Each energy harvesting element (recall the user specified configuration defined by 'd' in section 4.1.1) is assigned a range of "base" natural frequencies (i.e. the natural frequency of the energy harvester at day zero and at room temperature). At each time step, the current time and operating temperature are used to interpolate the effective Young's Modulus (recall Figure 4) and calculate the "current" natural frequency of each harvester; the representative acceleration profile for the current time step is also determined.

Looping over all possible global production tube rotations, the angular location of each energy harvesting element ($\alpha + \theta$) is determined (see Figure 7). Using this angle and the "current" natural frequency of each harvester, the signal power driving each harvester is determined (recall Figure 6). This looping sequence is continued for each harvesting element until signal power estimates are generated over the time domain of interest for each base frequency and over all thirty-six global rotation angles.

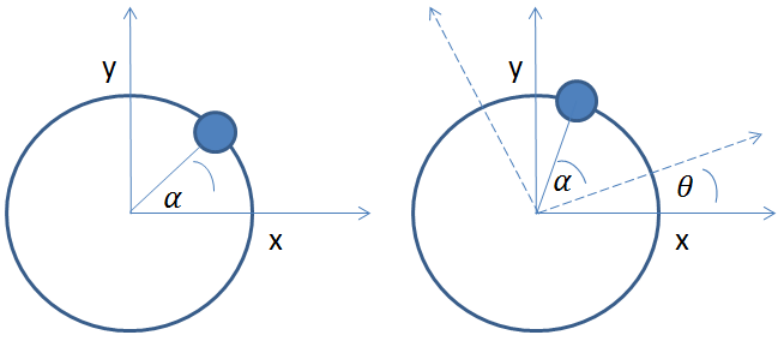

Figure 7. Global rotation

The power coefficient (units of m^2/s^3) for each realization is taken as

$$P(time, \theta, f_{EH1}, \dots, f_{EHn}) = \sum_{i=1}^{n} \frac{P_{signal}(time,\theta,f_{EHi})}{\omega_{n.current}}, \quad (4)$$

where the left hand side represents the combined power coefficient of a given realization at a given time, global rotation angle (θ), and base natural frequencies f_{EHi} for n user defined harvesting elements. A scalar estimator is calculated by numerically integrating the time-dependent power coefficient for each realization (i.e. for each fixed combination of $\theta, f_{EH1}, \dots, f_{EHn}$). This scalar is used to compare each combination of element base frequencies to determine the optimal set of base frequencies for the user defined configuration and at each global rotation angle. If the global rotation angle cannot be specified (perhaps due to installation uncertainties), an expected power coefficient is calculated by averaging the power coefficients from all thirty-six rotation angles and integrating as previously described. The output consists of optimal base frequencies for all n energy harvesting elements for a given global rotation angle and user specified configuration.

A power estimate (mW) is generated through the use of a viscous damping model. Using an uncoupled single degree of freedom (SDOF) lumped mass model, the energy extracted by the energy harvester is equated to energy dissipated by a viscous damping mechanism. Thus the model incorporates both a 'mechanical' and an 'electric' damper. While the unmodified SDOF model may prove inaccurate when compared to an Euler-Bernoulli beam model, a correction factor can be included to increase the accuracy of the SDOF model[10]. In the current phase, this modified SDOF model is preferred over other models (such as a coupled distributed parameter model) as it requires few inputs. The equation of motion for the modified lumped mass model can be written as[11]

$$m_{eq}\ddot{z} + c_{eq}\dot{z} + k_{eq}z = -m_{eq}\mu_1\ddot{y}. \tag{5}$$

The equivalent mass (m_{eq}) is written as[10]

$$m_{eq} = \frac{33}{140}M_b + M_t, \tag{6}$$

and is a function of the beam mass (M_b) and tip mass (M_t). Comparing equation (5) to an unmodified SDOF equation of motion, the correction factor (μ_1) is seen to scale the acceleration magnitude. The correction factor is written as[10]

$$\mu_1 = \frac{\left(\frac{M_t}{M_b}\right)^2 + 0.603\left(\frac{M_t}{M_b}\right) + 0.08955}{\left(\frac{M_t}{M_b}\right)^2 + 0.4637\left(\frac{M_t}{M_b}\right) + 0.05718}, \tag{7}$$

and is seen to converge to unity as the ratio of tip mass to beam mass increases. The correction factor can be used to modify previously-derived power estimates[12,13] to generate improved power estimates based on the modified SDOF lumped mass model. The normalized power extracted by each energy harvesting element is written as

$$P_{e\,max} = \frac{m_{eq}(\mu_1 A_n)^2}{16\omega_n\zeta_m} = \frac{m_{eq}{\mu_1}^2}{8\zeta_m}\left[\frac{{A_n}^2}{2\omega_n}\right] = \frac{m_{eq}{\mu_1}^2}{8\zeta_m}\left[\frac{P_{signal}}{\omega_n}\right], \tag{8}$$

where the driving acceleration time history has been deconstructed into to a single term Fourier series with (a) the driving frequency set to the "current" natural frequency of each energy harvester and (b) the acceleration magnitude (A_n) extracted from the corresponding signal power as $A_n = \sqrt{2P_{signal}}$. This implicitly assumes that driving accelerations not matching the "current" natural frequency of a given harvesting element provide negligible contribution to the total harvested energy. Note also that the derivation of equation (8) assumed that $c_{eq} = c_m + c_e$ and, further, that $c_m = c_e$.

As an illustration, consider the design of a three element energy harvester (α = 40°, 120°, 350°), oriented at a global rotation angle of 70° from the x-axis, and optimized from year 2.5 to year 4.5. The equations used to define the input acceleration time histories are shown in Appendix B with other inputs shown in Figure 3 and Figure 4. The optimal "base" natural frequencies are found to be 21Hz, 13Hz, and 19Hz, respectively. Assuming a tip mass of 0.010kg and a beam mass of 0.004kg for each of the three energy harvesting elements, the damping-normalized power output for each harvester can be determined (see Figure 8). The transition at year 3.5 is due to the change in representative acceleration

profile while the change at year 4.0 is due to the jump in expected operating temperature. The total output from the harvester configuration can be determined by adding the contributions from the individual energy harvesters. The total damping-normalized power estimates for four different mass realizations are shown in Figure 9 while the actual power estimates for a single mass realization (accounting for different damping ratios) are shown in Figure 10.

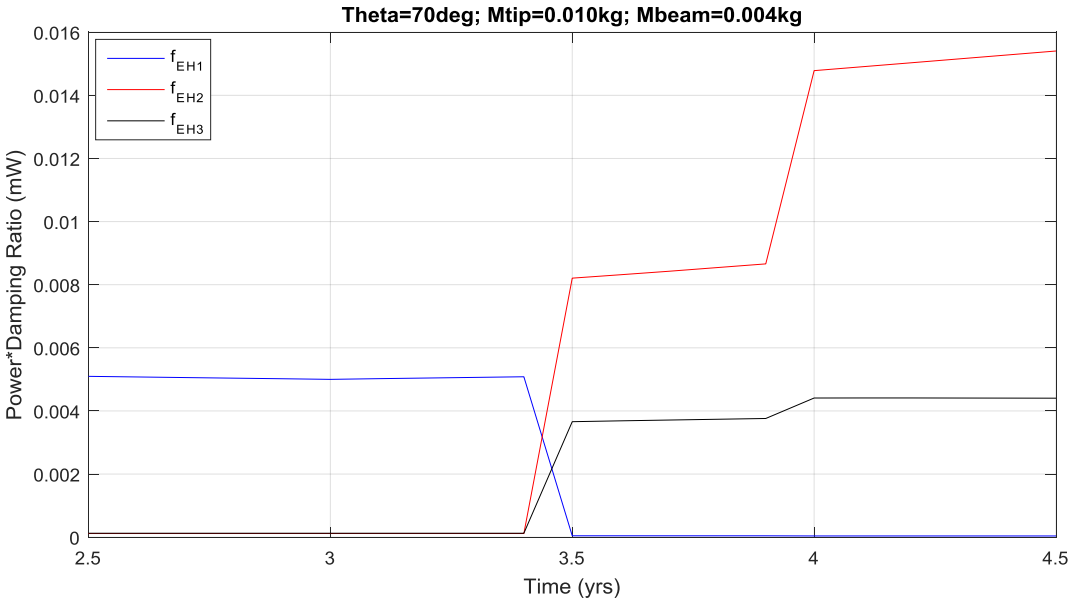

Figure 8. Damping-normalized power estimate for three individual energy harvesters

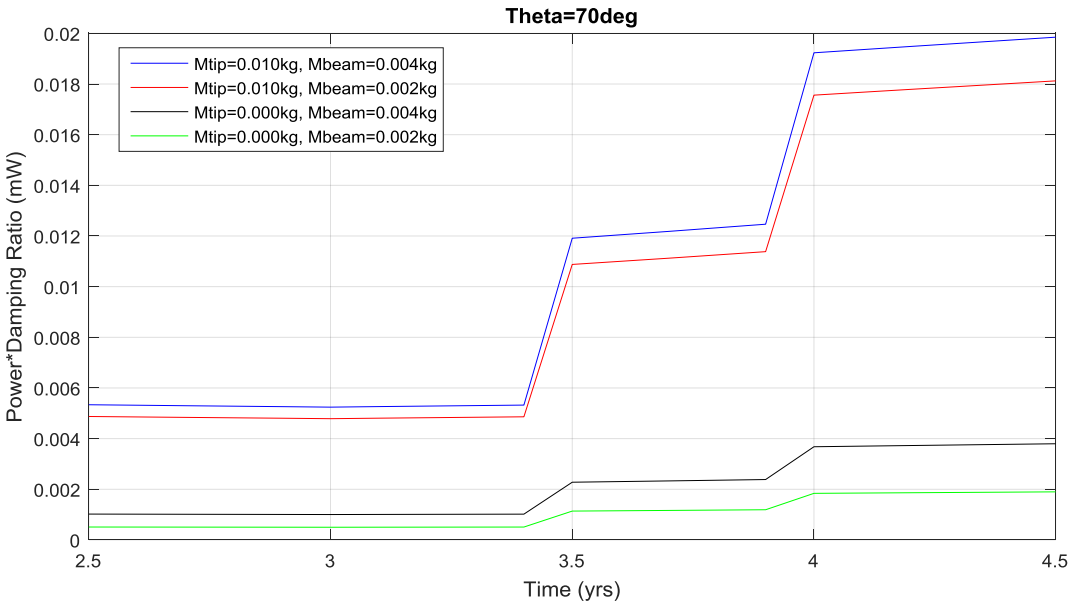

Figure 9. Total damping-normalized power estimate for four mass realizations

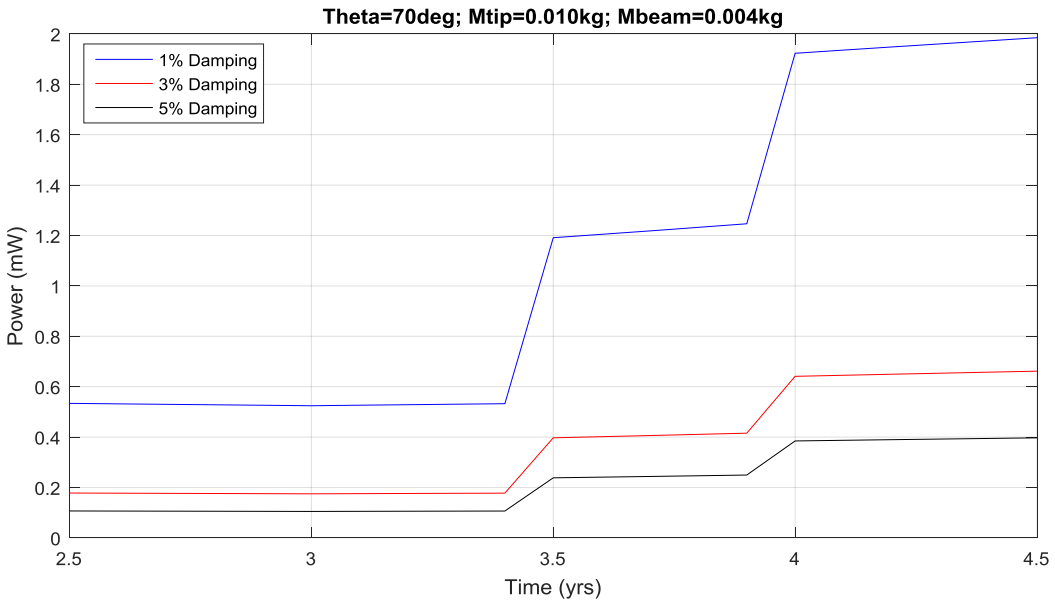

Figure 10. Power estimate for a single mass realization

5. FUTURE WORK

5.1 Phase two – refined power estimate

Using the optimal "base" frequencies calculated in phase one, the user can select commercially available piezoelectric elements for use in a refined analysis. After selecting specific piezoelectric elements, a more accurate power estimate can be generated using a coupled distributed parameter model[11]. In addition, the power estimate can include confidence intervals to account for uncertainty in the material and operating conditions. For example, the Young's Modulus may be difficult to predict after several years in service as stiffness degradation will vary depending on the number of cycles and amplitude of the tip displacement. By including uncertainty bounds on the Young's Modulus and other key inputs, a Monte Carlo analysis can be performed and power estimates can be generated based on user-defined confidence intervals.

5.2 Additional future work

After completing phase two of the program, other future work includes:

a. *Verifying the MATLAB generated power estimates.* Physical experimentation should be undertaken to verify the phase one and phase two power estimates. To this end, two experimental setups will be used. In the first setup, individual piezoelectric energy harvesters will be fixed to a unidirectional shake table and be subjected to known acceleration time histories. In the second setup, depicted in Figure 11, a structural housing will be fixed to a PVC representation of a hydrocarbon well. The "production tube" will be subjected to white noise, exciting the piezoelectric elements with colored noise. In both setups, the measured accelerations will be used as inputs in the MATLAB program; the power estimates will be compared to the experimental power outputs to verify the MATLAB programs functionality.

b. *Develop circuitry and storage devices.* To complete the design of a useable energy harvesting system, the energy extracted by the piezoelectric elements must be used to charge a power storage device. The necessary circuitry must be designed and a suitable storage device selected/designed.

c. *Obtain actual downhole acceleration time histories.* The amount of energy that can be harvested is a direct function of the production tube's acceleration time history. Actual time histories must be obtained to understand the magnitude and frequency profile for producing wells, permitting realistic power estimates to be made.

d. *Improve the structural housing design.* The design of the structural housing can be improved to (1) reduce local stress concentrations and (2) provide increased accessibility for real-world use.
e. *Fabrication and field testing of the energy harvesting system.* Once the structural housing/energy harvesting system is fabricated an industry partner is needed to enable in-situ testing. Field testing may need to be limited to test-wells to find a willing industry partner.

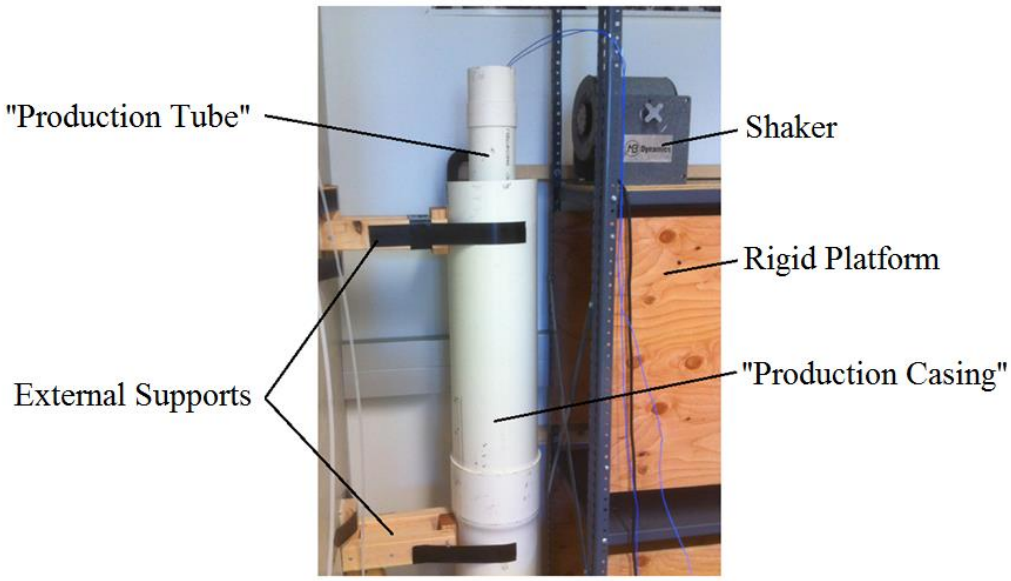

Figure 11. Experimental configuration

6. SUMMARY

A three-phase study was undertaken to determine the feasibility of a vibration based downhole energy harvesting system. In the first phase, analytical models were used in parametric studies to understand how high uncertainty variables affected the natural frequency and damping ratio of producing hydrocarbon. In the second phase, a structural housing was designed to meet targeted design pressures under load cases defined by the American Petroleum Institute. This preliminary design defined the radial width and volume in which the energy harvesting system will be placed. In the last phase, a software program was written in MATLAB to enable users to generate well-specific estimates of the harvestable power from a specific energy harvester configuration. Future work includes expanding and verifying the MATLAB software, developing a power storage system, and field testing a prototype.

ACKNOWLEDGEMENTS

Funding was provided by Los Alamos National Laboratory through the Engineering Institute under Task 5 (Subcontract No. 77137-001-11).

REFERENCES

[1] Kjolsing, E. and Todd, M., "A frequency study of a clamped-clamped pipe immersed in a viscous fluid conveying internal steady flow for use in energy harvester development as applied to hydrocarbon production wells." Proc. SPIE 9435, 943505 (2015).
[2] Kjolsing, E. and Todd, M., "The impact of boundary conditions and fluid velocity on damping for a fluid conveying pipe in a viscous fliud" SPIE Smart Structures/NDE (2016).
[3] Doyle, J. F., [Wave propagation in structures], Springer, US, (1989).
[4] Lee, U., [Spectral element method in structural dynamics], John Wiley & Sons, Asia, (2009).

[5] Païdoussis, M.P. and Issid, N.T., "Dynamic stability of pipes conveying fluid," Journal of Sound and Vibration 33(3), 267-294 (1974). .
[6] Stokes, G.G., [On the effect of the internal friction of fluids on the motion of pendulums, Vol. 9.], Pitt Press, (1851).
[7] Rosenhead, L., [Laminar boundary layers], Clarendon Press, Oxford, (1963).
[8] Wambsganss, M.W., Chen, S.S., and Jendrzejczyk, J.A., "Added mass and damping of a vibrating rod in confined viscous fluids," NASA STI/Recon Technical Report N 75, 10349 (1974).
[9] American Petroleum Institute (API), "Bulletin 5C3 – Formulas and calculations for casing, tubing, drill pipe, and line pipe properties," (1985).
[10] Erturk, A. and Inman, D.J., "On mechanical modeling of cantilevered piezoelectric vibration energy harvesters," Journal of Intelligent Material Systems and Structures, (2008).
[11] Priya, S. and Inman, D.J., [Energy harvesting technologies], Springer, US, (2009).
[12] Williams, C.B. and Yates, R.B., "Analysis of a micro-electric generator for microsystems," Sensors and Actuators A 52 (1), 8-11 (1996).
[13] Roundy, S., Wright, P.K., and Rabaey, J., "A study of low level vibrations as a power source for wireless sensor nodes," Computer communications 26(11), 1131-1144 (2003).

APPENDIX A - NOMENCLATURE

The terms used in this manuscript are listed in Table A.1.

Table A.1. Nomenclature

Dimensional Terms

a_{normal}	Acceleration in the Normal Direction
$a_{tangential}$	Acceleration in the Tangential Direction
a_x	Acceleration in the Global X-Direction
a_y	Acceleration in the Global Y-Direction
c	Viscous Damping Coefficient
c_e	Electric Damping Coefficient
c_{eq}	Equivalent Damping Coefficient
c_m	Mechanical Damping Coefficient
d	Pipe Outer Radius
f_{EH}	Energy Harvester Base Frequency
f_{hydro}	Hydrodynamic Force
g	Coefficient of Gravity
k_{eq}	Equivalent Stiffness
m	Mass per Unit Length of Pipe
m_{eq}	Energy Harvester Equivalent Mass
n	Number of Harvesting Elements
$\bar{p}$	Mean Pressure Differential
w	Lateral Deflection of the Pipe
y	Base Displacement
z	Relative Displacement
A_i	Flow Area
A_n	Magnitude of Acceleration
D	Confining Shell Inner Radius
E	Young's Modulus
E^*	Kelvin-Voigt Viscosity
I	Pipe Inertia

Dimensional Terms (cont.)

K_r	Rotational Spring Stiffness
M_b	Beam Mass
M_i	Mass per Unit Length of Conveyed Fluid
M_t	Tip Mass
P	Power Estimate
$P_{e\,max}$	Estimate of Harvested Electrical Power
P_{signal}	Signal Power
$\bar{T}$	Externally Applied Tension
U	Mean Axial Flow Velocity
$U_0 e^{i\omega t}$	Pipe Velocity
α	Harvester Location with Zero Global Rotation
θ	Global Rotation Angle
ρ_e	Annulus Fluid Density
υ_e	Annulus Fluid Kinematic Viscosity
ω	Radial Frequency
ω_n	Natural Frequency

Dimensionless Terms

i	Imaginary Unit
ζ	Equivalent Damping Ratio
ζ_m	Mechanical Damping Ratio of Harvesting Element
μ_1	Correction Factor
ν	Poisson Ratio
Γ	Hydrodynamic Function
Γ_i	Imaginary Part of the Hydrodynamic Function
Γ_r	Real Part of the Hydrodynamic Function

APPENDIX B – ACCELERATION PROFILES

Acceleration profile #2:

$$a_x = 1.5\sin(2\pi * 14Hz * t) + 1.5\sin(2\pi * 25Hz * t) + 0.7\sin(2\pi * 40Hz * t) + Uniform\ Noise\ [-3,3]\ \left(\frac{m}{s^2}\right) \quad \text{(B.1)}$$

$$a_y = 1.5\sin(2\pi * 10Hz * t) + 1.0\sin(2\pi * 20Hz * t) + 1.0\sin(2\pi * 35Hz * t) + Uniform\ Noise\ [-3,3]\ \left(\frac{m}{s^2}\right) \quad \text{(B.2)}$$

Acceleration profile #3:

$$a_x = 1.7\sin(2\pi * 12Hz * t) + 1.0\sin(2\pi * 22Hz * t) + 0.5\sin(2\pi * 28Hz * t) + Uniform\ Noise\ [-3,3]\ \left(\frac{m}{s^2}\right) \quad \text{(B.3)}$$

$$a_y = 0.9\sin(2\pi * 18Hz * t) + 0.8\sin(2\pi * 25Hz * t) + 0.6\sin(2\pi * 50Hz * t) + Uniform\ Noise\ [-3,3]\ \left(\frac{m}{s^2}\right) \quad \text{(B.4)}$$